Available online at www.sciencedirect.com
SCIENCE DIRECT®
Journal of Catalysis 223 (2004) 309–318
JOURNAL OF CATALYSIS
www.elsevier.com/locate/jcat

The effect of surface-active carbon on hydrocarbon selectivity in the cobalt-catalyzed Fischer–Tropsch synthesis

Christopher J. Bertole,[a,1] Gabor Kiss,[b] and Charles A. Mims [a,*]

[a] *Department of Chemical Engineering and Applied Chemistry, University of Toronto, Toronto, ON M5S3E5, Canada*
[b] *ExxonMobil Research and Engineering Company, Corporate Strategic Research Laboratories, 1545 Rte 22E, Annandale, NJ 08801, USA*

Received 9 October 2003; revised 5 January 2004; accepted 2 February 2004

Abstract

Carbon isotope transients ($^{12}CO \rightarrow {}^{13}CO$) at reaction steady state were used to correlate the in situ surface inventories of active carbon species with product selectivity variations in the Fischer–Tropsch synthesis. The measurements were conducted on an unsupported cobalt catalyst at a variety of elevated pressure conditions (syngas pressures from 3 to 15 atm, H_2:CO ratios from 1 to 4, temperatures from 190 to 228 °C, and cofed water vapor pressures from 0 to 8 atm). The in situ adsorbed CO inventory is saturated and insensitive to the changes in reaction conditions, except for a small decrease in the presence of elevated water pressures. A large amount of active carbon intermediates is present as a monomeric species on the catalyst, and this amount varies widely with reaction conditions (adsorbed C^*/CO values from 0.3 to 0.8). Changes in active carbon inventory cause proportional changes in the polymerization probability at all carbon numbers. For the most part, carbon monoxide and water influence the polymerization probability indirectly by causing changes in the monomer C^* amounts. Hydrogen and temperature do not cause significant changes in monomeric carbon, but influence the rate coefficients directly. The influences of gas composition on the rate coefficients provide useful information regarding the site requirements for chain growth.

Keywords: Fischer–Tropsch synthesis; Cobalt catalyst; Isotope transient; Kinetics; Active carbon; Surface inventory; Selectivity

1. Introduction

Selectivity in the Fischer–Tropsch synthesis (FTS) is a central issue concerning its use in such processes as the conversion of stranded natural gas reserves to liquid fuels [1–9]. Reaction conditions have an important effect on product selectivities in FTS. High temperatures and H_2:CO feed ratios are associated with higher methane selectivity, lower probability of hydrocarbon chain growth, and lower olefinicity in the products [4,7,9–11]. Conversely, the addition of water vapor, a major product of the reaction, can have the opposite effects on selectivity [7,12–29]. Despite years of investigation, it is not clear how reaction conditions affect the amounts and reactivities of the surface intermediates that are responsible for the observed selectivity patterns. This paper reveals the hidden effects of reaction conditions on a major surface intermediate, monomeric active carbon.

The selectivity pattern in FTS mechanism is dominated by a complex surface polymerization mechanism [4,7,9,30–32]. The dominant hydrocarbon products are generally believed to result from growth of alkyl species by reaction with methylene monomers [9,30–42]. Although the FTS product distribution is dominated by 1-alkenes and *n*-alkanes, minor products such as double-bond and branched isomers and oxygenates result from distinct reaction steps [7,31]. The polymerization reaction is partially reversible. CO–alkene cofeed experiments have shown that 1-alkene primary products can readsorb on Co, Ru, and Fe catalysts, serving as initiators for further polymerization [43–55] as well as depolymerization [50–52,55]. Variations of the polymerization probability with carbon number produce irregularities in the production distribution. The polymerization probability is typically lowest for C_1, exhibits a local maximum for C_2, and generally increases through the medium (C_7–C_{15}) molecular weight product range. Alkene readsorption plays a significant role in this behavior; hence current detailed re-

* Corresponding author.
E-mail address: mims@chem-eng.utoronto.ca (C.A. Mims).
[1] Current address: Cormetech, Inc., 5000 International Drive, Durham, NC 27712, USA.

0021-9517/$ – see front matter
doi:10.1016/j.jcat.2004.02.001

action models include alkene readsorption effects together with multiple termination paths (alkane, alkene, isomerization, branching) to explain the full complexity of the product distribution [4,7,45,56–58]. Multiple site explanations have also been offered [59–64] for some of these complexities. Mass transport issues have a strong influence on the degree to which readsorption modifies the product distribution [7, 47,48,57] and can also be responsible for some observed variations from catalyst to catalyst. Despite the many thorough studies directed toward FT selectivity, these issues are still vigorously debated and thus warrant further investigations.

The polymerization probabilities depend on the surface concentrations of intermediates, particularly that of the monomer. The monomer concentration is a "hidden variable" governing the reaction selectivity that is not a trivial function of reaction conditions. In a simple model of the polymerization process, the probability of further growth at carbon number n is determined by the competition between chain growth,

$$C_n^* + C_m^* \rightarrow C_{n+1}^* \quad (1)$$

and termination to produce stable products,

$$C_n^* \rightarrow C_n. \quad (2)$$

An asterisk denotes a surface-bound species or process, and the subscripts denote the carbon number $(n, n+1)$ or monomer (m). The C_n^* surface growth probability, α_n^*, is given by the ratio of the growth (g) and termination (t) rates [9], i.e.,

$$r_{g,n}^*/r_{t,n}^* = \alpha_n^*/(1-\alpha_n^*). \quad (3)$$

If the polymerization step obeys mass action surface rate laws, the surface growth/termination rate ratio is given by

$$r_{g,n}^*/r_{t,n}^* = k_{g,n}^*\theta_{C_m^*}\theta_{C_n^*}/k_{t,n}^*\theta_{C_n^*} = (k_{g,n}^*/k_{t,n}^*)\theta_{C_m^*}, \quad (4)$$

where $\theta_{C_m^*}$ and $\theta_{C_n^*}$ are the surface fractional coverages by the monomer species and the C_n^* growing chain, respectively. The rate coefficients, $k_{g,n}^*$ and $k_{t,n}^*$, contain other dependencies on surface composition (open sites, adsorbed hydrogen, etc.). This simple kinetic treatment shows that a change in hydrocarbon chain growth probability can arise either (1) from a change in the rate coefficient ratio, $k_{g,n}^*/k_{t,n}^*$, or (2) from a change in the monomer coverage $\theta_{C_m^*}$. The monomer surface concentration is controlled indirectly by a dynamic balance between the rate of formation and consumption, *not* directly by reactant or product partial pressures. Therefore, it must be measured in situ in order to reveal its role in selectivity changes.

Isotope transient studies at reaction steady state [15,23, 28,65–78] have shown that the metal surfaces of working FT catalysts (Co, Fe, and Ru) are crowded with adsorbed species. Some of these surface species arise from the reversible adsorption of molecular reactants (CO and H_2) and products (H_2O and olefins). Others are governed by the dynamic balance between their rate of formation from the reversibly adsorbed species and their consumption in essentially irreversible surface reactions. Previous $^{12}CO \rightarrow {}^{13}CO$ isotope transients at reaction steady state have shown the following:

1. The surface carries a saturated amount of adsorbed CO, which is rapidly exchanged with the gas phase [65–70]. Simultaneously, the surface carries a substantial amount of transient (reactive) carbon-containing intermediates, C^*.
2. Once initiated, chain growth occurs rapidly compared to the lifetime of the average monomer on the surface [65–70,73]. As a consequence, the growing hydrocarbon chains cover a very small fraction of the available surface, unless the process is largely reversible [67], while the majority of the active carbon inventory, C^*, is in monomeric form.

Although previous isotope transient studies on cobalt FTS have revealed the major reaction paths, they have not systematically investigated the effects of reaction conditions on the amounts of carbon intermediates present on the catalyst surface nor have these measurements been made under industrially relevant high-pressure conditions. This paper addresses some of these issues, using carbon isotopic transients ($^{12}CO \rightarrow {}^{13}CO$) to demonstrate the subtle interplay between surface intermediates and product selectivity. The transients were measured at a variety of temperatures, and reactive gas compositions (hydrogen, carbon monoxide, and water) in order to separate the effects on $k_{g,n}^*/k_{t,n}^*$ from changes in the amounts of active carbon species.

2. Experimental

The reactor, described previously [15,79], is a down-flow, tubular (4 mm i.d.), fixed bed. All feed and effluent lines, and the reactor, are housed in a hotbox held at 190 °C to prevent steam condensation. It is capable of operating at up to 28 atm total pressure and allows cofeeding of steam. The steam is generated in the hydrogen stream by adding the required amount of extra hydrogen and a stoichiometric amount of oxygen and then contacting this mixture with a heated Pt catalyst just prior to mixing with the CO/tracer stream. A trap placed on the CO feed line (TiO_2 pellets, 320 °C) prevents contamination by metal carbonyls. The reaction temperature is measured by a sheathed thermocouple positioned in the center of the catalyst bed. The on-line GC (HP5890 with FID and a 60 m Supelco SPB-1 column) measures hydrocarbons (paraffins and olefins) from C_1 through C_{22}. Due to concerns about condensation in the product line, product rates through only C_7 were used in this study. CO conversions were determined by GCMS from mass balances based on a premixed Ne internal standard. CO_2 production rates were also mea-

sured by GCMS. The carbon-based C_{8+} production rate was given by difference between the total CO reaction rate and the production rates of the measured carbon-containing products. The isotope transient experiments were performed by switching ^{13}CO/Ar (in a fixed volume loop isobaric with the feed) for ^{12}CO/Ne in the feed. On-line MS (Balzers QMS420) monitored the isotope transients in addition to being used for GCMS analysis.

We used an unsupported cobalt catalyst for these experiments to avoid possible complications from support effects. Rhenium was present in this catalyst (Re/Co = 0.03), since it is known to enhance cobalt reduction (and dispersion) for supported cobalt catalysts [80]. Our previous studies [78] showed that the presence of rhenium on supported catalysts affects neither the steady-state catalyst performance nor the isotope transient behavior. The catalyst charge in the reactor (0.30 g, 180- to 250-μm particles) was diluted with SiC (0.23 g, Strem, 150 μm) to assure isothermality. The length of the catalyst bed was approximately 10 mm. Particle size-dependent measurements [79] on supported catalysts with 10 times higher volumetric reactivity indicate that our unsupported catalyst was unaffected by mass-transfer limitations on the reactants over the full range of reaction conditions.

The unsupported catalyst was reduced under flowing hydrogen at ambient pressure while the temperature was first raised at 0.4 °C/s to 250 °C, held at this temperature for 12.5 h, and then cooled. The low reduction temperature prevented the bulk metal catalyst from extensive sintering. Syngas feed was introduced when the reactor reached 200 °C; followed by gradual increases in reactor pressure and temperature (1 °C/min) to the desired conditions. There was a negligible pressure drop under the high-pressure reaction conditions. The catalyst was on syngas for 3 days before the start of the rate measurements and isotope transients. During this time, a small (∼30%) decrease in activity and a reduction in methane selectivity were noted.

After the line-out time, isotope transients and rate data were collected for the reaction conditions listed in Table 1.

Table 1
Reaction conditions for the isotopic transient experiments (units: temperature in °C, pressure in atmospheres)

	P_{CO}				
P_{H_2}	1	1.25	2.5	4	5
2	210 (0,8)				
2.5		200 (0)	210 (0)		
5		200 (0)	210 (0,4)		210 (0)
5		210 (0,4)			221 (0)
5					228 (0)
8				210 (0)	
10			200 (0)		210 (0)
10			210 (0,4)		221 (0)
10			221 (0)		

Each combination of H_2 (row) and CO (column) partial pressures was investigated at the temperatures indicated in the table. The numbers in parentheses indicate the water feed vapor pressures that were studied for each H_2:CO:T combination

By adjusting space velocity, the CO conversion was held in all cases at 11 ± 1%. After each change in the reaction condition, the reaction was allowed to reach steady state (usually 1–2 h) and then run for another 1–2 h before the isotope transient experiment was performed. Both the forward and the reverse isotopic transients were measured for each experiment. Over the course of the catalyst run, which took 17.5 days to complete, a few of the conditions were examined more than once. Periodic returns to one particular standard condition (210 °C, $P_{H_2} = 10$ atm, $P_{CO} = 5$ atm, $P_{inert} = 8$ atm, CO conversion = 11 ± 1%) were used to track any irreversible changes in catalyst performance. Following the full series of dry experiments, a smaller set of experiments with cofed water vapor was performed (also with interspersed activity checks under the standard conditions).

A typical isotope transient is shown in Fig. 1. The reversibly adsorbed CO inventory (N_{CO}) is determined by the amount of ^{12}CO displaced from the catalyst after the isotope switch (shown in the figure). Fig. 1 also shows the washout curve for ^{12}C in the methane product from which we obtain the methane time constant (τ_{CH_4}). This curve (and all the other transients in this study) can be well reproduced by convoluting a single exponential decay over the isotope decay function measured in the CO. As has been previously reported [67,73], the methane time constant is very similar to the decay of ^{12}C in all the hydrocarbon products (i.e., $\tau_{C^*} = \tau_{CH_4}$). The total amount of carbon (N_{C^*}) contained in active surface intermediates is thus given by multiplying the CO reaction rate (minus the CO_2 production rate) by the methane time constant. Methane is the preferred hydrocarbon to measure the kinetics of C* removal since it is easily

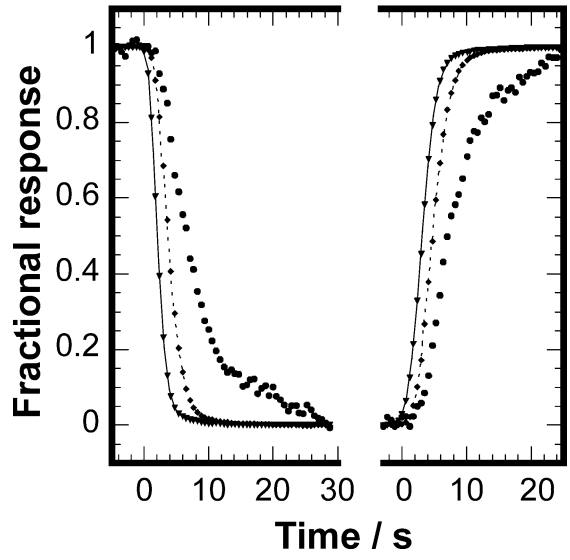

Fig. 1. Sample isotope transient on the unsupported catalyst at 210 °C, syngas pressure = 15 atm, H_2:CO = 2:1. Solid line and inverted triangles, Ne tracer in ^{12}CO stream; dashed line and diamonds, ^{12}C fraction in CO; solid circles, ^{12}C fraction in methane. Both the forward (^{13}CO → ^{12}CO, left), and reverse (^{12}CO → ^{13}CO, right) transients are shown.

measured by mass spectrometry. It is also the least susceptible of the hydrocarbon products to further hold up in the reactor due to mass transport or high solubility in the resident liquid product.

3. Results and discussion

3.1. Data

The reaction rates, selectivities, and the measured amounts of adsorbed C* and CO are collected in Table 2. A letter label (column 2) is assigned to each H_2/CO pressure (P_{H_2}/P_{CO}) combination (the data are grouped for determining temperature dependence); a "w" suffix is added when water was cofed. The experiments are arranged in the table according to these reaction conditions (first by increasing temperature and secondarily by syngas composition). The chronological order is indicated by the experiment run numbers in column 1 (this information allows the reader to assess the effectiveness of the bracketing experiments, and understand the discussion of deactivation due to water vapor). Results from multiple measurements under given conditions are listed in the table as averaged values. The reproducibility (indicated by the standard deviations for condition "f") is consistent with independent error estimates. Various features of the data are briefly discussed next before examining the role of C* in the selectivity variations.

3.1.1. Activity maintenance

Periodic activity checks (under the standard condition "f") showed no measurable changes to the catalyst during the entire sequence of dry experiments. The averaged results under this condition, along with standard deviations, are shown in Table 2 and thus represent the (constant) properties of the catalyst just prior to the steam addition experiments. Cofed water induced significant reversible and irreversible changes to the catalyst. These changes were tracked with activity checks performed under the dry standard condition, and the turnover frequencies in Table 2 were corrected for deactivation by a procedure explained in Ref. [15]. Water caused a substantial decrease in catalyst activity but selectivity was unaffected.

3.1.2. Selectivities

In addition to carbon-based selectivities to methane and carbon dioxide, two calculated values of chain growth probability for the higher hydrocarbons are shown in Table 2. These values use the well-known Anderson–Schulz–Flory (ASF) product distribution [9,32], which is obeyed if the chain growth probability is constant. The first parameter, α_{5-7}, is derived from the measured product ratios in the C_5–C_7 region, and the second value, α_{8+}, is the value of an ASF distribution that would give the measured C_{8+}/C_5-C_7 carbon-based product ratio. The uncertainties in the calculated molar C_{8+} production rates are estimated to introduce a 5% uncertainty in the calculated values of $r^*_{g,n}/r^*_{t,n}$ presented later. The data indicate that the value of α_{8+} is higher than that for the C_5–C_7 range, suggesting an increase in α with carbon number beyond C_7. This is consistent with more complete product characterization results under similar reaction conditions [7]. These previous studies showed that beyond C_{10}, the product distribution is well represented by an ASF distribution with a somewhat higher value of α than the value that characterizes the C_5–C_7 region. Table 2 shows that the two values correlate well with each other and both anticorrelate with methane selectivity.

3.1.3. Surface chain growth probabilities, α^*_n

The ratio $r^*_{g,n}/r^*_{t,n}$, and therefore α^*_n for each carbon number product can be obtained from the following expression [81]:

$$r^*_{g,n}/r^*_{t,n} = \Bigg(\sum_{m=n+1,\infty} r_m\Bigg)\Big/ r_n. \tag{5}$$

In order to evaluate the sum in the numerator of Eq. (5), we estimated the (unmeasured) molecular based C_{8+} rates from the carbon-based C_{8+} selectivities by assuming an ASF distribution for $n > 7$. Values of α^*_n, calculated from the resulting values of $r^*_{g,n}/r^*_{t,n}$ are shown in Fig. 2 for two of our conditions. They are in accord with published chain growth parameters under similar conditions, two of which are shown in Fig. 2.

3.1.4. Alkane–alkene selectivities

The molar-average alkane fractions in the C_2–C_7 products are indicated for each condition (Table 2) and for each carbon number (Fig. 3). The C_2 products are dominated by ethane, whereas the higher carbon number products are dominated by alkenes. A trend toward higher alkane fractions is observed as the carbon number increases from 3 to 7. This trend has been previously associated with readsorption of primary alkene products followed by further molecular weight growth. A finite probability of alkane formation with each visit to the surface produces trends like those seen in Fig. 3 [7,57].

3.1.5. Isotope transients: Adsorbed CO

Under dry feed conditions, the catalyst held an average of 3.1 molecules of adsorbed CO per thousand cobalt atoms. This amount did not vary substantially with reaction conditions, although up to a 20% reversible decrease occurred in the water cofeeding experiments (see Table 2). The CO adlayer is essentially saturated under the conditions of this study and the CO/Co ratio provides a reasonable measure of the metal dispersion [77–79].

3.1.6. Isotope transients: C* coverages

Substantial steady-state amounts of active carbon, C*, are present under all reaction conditions. The values of the ratios of adsorbed C* to CO (C*/CO in Table 2) vary widely (from 0.3 to 0.8). Surprisingly, these large variations in the active

Table 2
Isotope transient experiments: Reaction conditions and selected results

Run No.	Condition[a]					Rates[b]		Selectivities[c]						Transient[d]			
		T	H_2	CO	H_2O	f_{CO}	$-r_{CO}$	CH_4	CO_2	C_{8+}	α_{5-7}	α_{8+}	f_{ane} (2–7)	CO/Co ($\times 10^3$)	k_{CO}	k_{C^*}	C^*/CO
19	a	200	5	1.25	–	0.105	0.151	0.119	0.010	0.697	0.82	0.899	0.48	2.8	0.049	0.097	0.504
26	b	200	10	2.5	–	0.108	0.166	0.096	0.007	0.712	0.83	0.899	0.37	3.1	0.054	0.106	0.506
18	a	210	5	1.25	–	0.115	0.167	0.156	0.011	0.601	0.80	0.869	0.47	3.1	0.054	0.141	0.381
4, 25	b	210	10	2.5	–	0.114	0.295	0.139	0.008	0.649	0.83	0.888	0.48	2.9	0.096	0.167	0.575
11	c	210	2	1	–	0.092	0.075	0.140	0.015	0.552	0.78	0.844	0.44	2.9	0.024	0.071	0.339
6	d	210	5	2.5	–	0.104	0.197	0.064	0.011	0.774	0.88	0.909	0.30	3.0	0.064	0.110	0.576
8	e	210	8	4	–	0.107	0.212	0.063	0.011	0.773	0.86	0.911	0.30	3.1	0.069	0.099	0.688
3, 7, 12, 15, 29[e]	f[e]	210	10	5	–	0.109	0.232	0.068	0.010	0.762	0.83	0.909	0.32	3.2	0.075	0.121	0.626
						±0.06	±0.02	±0.003	±0.002	±0.015	±0.02	±0.02	±0.02	±0.11	±0.007	±0.024	±0.061
9	g	210	2.5	2.5	–	0.096	0.110	0.040	0.010	0.832	0.88	0.920	0.22	2.8	0.036	0.049	0.714
31	aw	210	5	1.25	4	0.107	0.237	0.101	0.026	0.678	0.85	0.893	0.40	2.5	0.077	0.095	0.790
30	bw	210	10	2.5	4	0.090	0.241	0.068	0.022	0.754	0.84	0.911	0.34	2.9	0.078	0.103	0.745
37	cw	210	2	1	8	0.063	0.052	0.031	0.086	0.775	0.80	0.928	0.22	1.7	0.024	0.035	0.627
32	dw	210	5	2.5	4	0.108	0.177	0.040	0.028	0.822	0.84	0.925	0.27	2.5	0.058	0.070	0.800
13, 17, 21	a	221	5	1.25	–	0.112	0.245	0.243	0.014	0.409	0.75	0.813	0.56	3.3	0.079	0.203	0.387
24	b	221	10	2.5	–	0.118	0.417	0.186	0.009	0.553	0.78	0.864	0.53	3.4	0.135	0.251	0.534
14	h	221	5	5	–	0.103	0.246	0.044	0.011	0.819	0.86	0.924	0.25	3.3	0.080	0.121	0.655
22	h	228	5	5	–	0.088	0.352	0.054	0.010	0.801	0.84	0.916	0.25	3.4	0.114	0.148	0.763

[a] Temperatures in °C, feed partial pressures in atmospheres.

[b] f_{CO} is CO fractional conversion, r_{CO} is metal time yield in (mmol CO) (mol Co)$^{-1}$ s^{-1}; metal time yields for the water cofeeding experiments have been corrected for deactivation as described in the text and more detail in Ref. [15].

[c] Selectivities are carbon based, α_{5-7} is ASF chain growth probability based on measured C_5–C_7 products; α_{8+} is calculated from carbon-based selectivities, assuming an ASF distribution by the following expression: $S(C_{8+})/S(C_5\text{–}C_7) = \{(5-4\alpha_{8+})/[\alpha_{8+}^3(8-7\alpha_{8+})]-1\}^{-1}$; $f_{ane}(2\text{–}7)$ is the molar average alkane fraction in the C_2–C_7 products.

[d] CO/Co is mol CO adsorbed per mol bulk Co; k_{C^*} is the isotope decay constant in the methane product in s^{-1}; k_{CO} is CO conversion rate divided by the CO inventory in s^{-1}.

[e] Standard condition – error estimates equal one standard deviation.

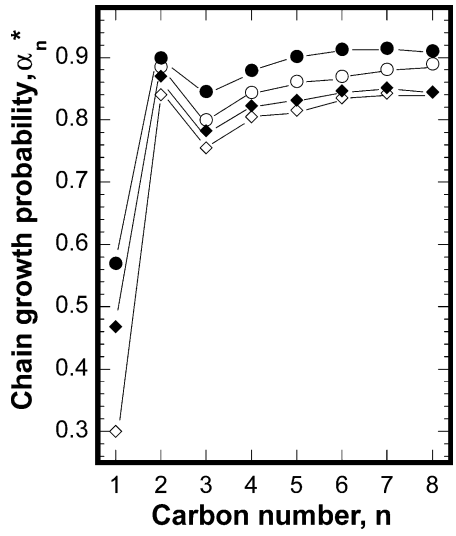

Fig. 2. Chain growth probability, α_n^*, versus carbon number. Closed symbols are experiments from the present study at 210 °C without added water in the feed: H_2:CO partial pressures = 10:5 (circles) and 5:2.5 (diamonds). Open circles are from Fig. 7 of Ref. [7] (low conversion data at 200 °C on Co/TiO_2). Open diamonds are 210 °C data at moderate (30%) CO conversion from Fig. 2, Ref. [45] (Co/ZrO_2/Kieselguhr).

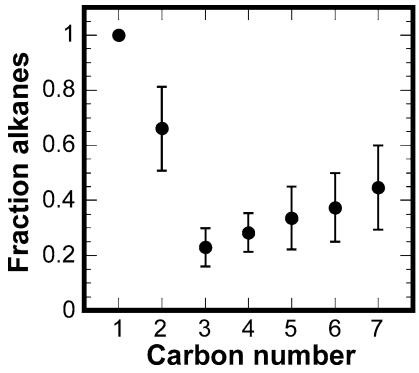

Fig. 3. Average molar alkane fraction as a function of carbon number for the experiments in Table 2. The bars represent ± one standard deviation.

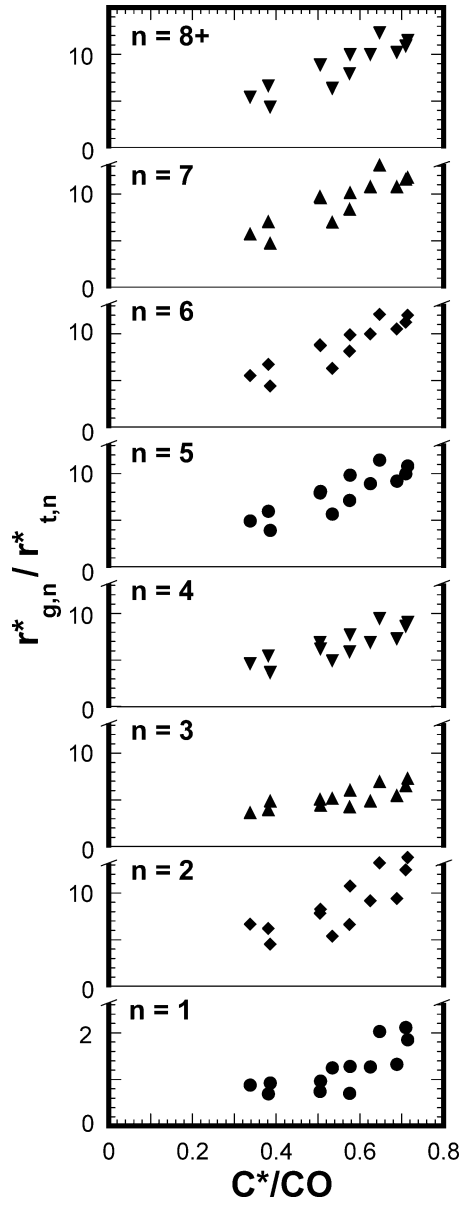

Fig. 4. Dependence of $r^*_{g,n}/r^*_{t,n}$ ratios (from Eqs. (3) and (5)) on the surface C* coverage (C*/CO ratio) for C_1 through C_7 stages of polymerization. All experiments from Table 2 are included except for those with cofed water.

carbon inventory had little or no effect on the CO inventory on the surface. This indicates that the two species do not compete for the same surface sites under these conditions. To the extent that the adsorbed CO measures the number of sites, the ratio C*/CO is a measure of the surface coverage by C*. Furthermore, since this carbon is monomeric, C*/CO is a measure of the monomer coverage, $\theta_{C^*_m}$, and we use these interchangeably in the following discussion. Since site loss occurred during wet feed experiment 37 (see Ref. [15]), the C*/CO value was calculated using CO/Co obtained in the subsequent dry activity check under the standard conditions.

3.2. Hydrocarbon growth probability: Effects of C*

3.2.1. General correlation with C*

A substantial portion of the selectivity changes are correlated with simultaneous changes in the amount of C*. The $r^*_{g,n}/r^*_{t,n}$ ratios for carbon numbers from 1 to 7 as well as those calculated for C_{8+} are shown as a function of the measured surface C*/CO ratio in Fig. 4. All experiments with dry feeds have been included and thus involve changes in hydrogen pressure, carbon monoxide pressure, and temperature. Each panel (i.e., each carbon number) shows a strong correlation of $r^*_{g,n}/r^*_{t,n}$ with C*/CO. Therefore, a substantial fraction of the variation in chain growth probability can be attributed to changes in the monomer inventory. The changes in C* amounts result indirectly from alteration of the dynamic balance between C* formation and its consumption. The residual variability not associated with C* must be attributed to changes in the rate coefficient ratio $k^*_{g,n}/k^*_{t,n}$. In the next section, we use regression analyses to determine

how each of the various reaction condition parameters (gas composition and temperature) is related to changes in C*.

3.2.2. Data regressions

The $r^*_{g,8+}/r^*_{t,8+}$ data (dry, no water cofeed) were fit to expressions which include power-law terms in θ_{C^*}, P_{H_2}, and P_{CO} and an Arrhenius term for the temperature dependence. The results of these regressions, along with the average fractional errors, are shown in Table 3. These findings can be corroborated qualitatively by a detailed inspection of the data in Table 2. The first entry (1) simply tabulates the standard deviation of the values of $r^*_{g,8+}/r^*_{t,8+}$ (33.8%) as a fraction of its mean value (7.97). A linear C* term alone (expression 2) is able to correlate a major fraction of this variability—the average fractional error is reduced to 16%. The optimized order in C* was 1.05, indistinguishable from a linear dependence. Gas-phase terms and temperature terms alone, without a C* term (expression 3), are capable of an even better fit with an average fractional error of 11%. This correlation shows the expected positive influence of CO and the negative influences of hydrogen pressure and temperature on chain growth. An expression containing all terms (C*, gas composition and temperature—expression 4) improves the fit to 7.9% average fractional error, a value near the experimental uncertainty. In fit 4, the gas-phase orders and temperature parameters represent the residual effects of the reaction conditions that cannot be explained by C* coverage changes. Of the full CO order (0.57), all but 0.16 is subsumed into the C* variations. On the other hand, a substantial portion (–0.16) of the overall (–0.20) order dependence in H_2 cannot be explained by C* changes. Finally, most of the temperature dependence (32 out of 39 kJ/mol) remains in fit 4, showing that, like hydrogen, only a small fraction of the decrease in chain growth with temperature can be assigned to changes in C*. A regression of C*/CO (θ^*_C) dependence on syngas composition and temperature provides $\theta_{C^*} = 0.118\exp\{650/T\}p_{H_2}^{-0.05}p_{CO}^{0.41}$. This expression is an indication of the effect of the reaction conditions on the amount of C* and, therefore, of the indirect effects of reaction conditions on selectivity changes.

If the water cofeed experiments are included, the complete expression (C*, gas composition and temperature) provides a somewhat poorer fit (12% average fractional error), but the residual gas phase and temperature dependencies are largely unchanged (see expression 5). The average value of $\Delta\ln(r^*_{g,8+}/r^*_{t,8+})/\Delta\ln(C^*/CO)$ is 0.95 for the four wet-dry pairs of experiments. Thus, as described in Ref. [15], the dominant effect of added water vapor on chain growth can be explained by changes in the amount of C*. Some, or all, of the effects of CO pressure determined above could be due to the effect of water. This arises from the fact that a fixed CO conversion was used in these experiments, thus producing a water concentration (in the dry feed experiments) in proportion to CO. In view of the effect of water, it is likely that all of the indirect (C* inducing) effects of CO seen in the regressions are due to parallel water pressure changes.

Chain growth for all of the carbon number products (C_1 through C_7) were analyzed using the same statistical procedure as above. These results show interesting trends, summarized in the three panels of Fig. 5. Figs. 5a, 5b, and 5c show the parameters relating to CO, H_2, and temperature, respectively. The circles result from fits which include only CO, H_2, and temperature terms without a C* dependence, and these represent the full apparent gas-phase and temperature dependence of $r^*_{g,n}/r^*_{t,n}$. The diamonds result from fits which include a linear C* term and represent the residual dependencies that cannot be correlated by C* variations alone. The effects of the parameters on θ_{C^*} are indicated by the dashed lines.

Asymptotic behavior is observed for C_5 and heavier products, which agrees with the parameters obtained for the C_{8+} products above. In this limit, increasing CO pressure causes an increase in chain growth probability (roughly 0.5 order), but a major portion of this (0.4 order) is explained by the simultaneous C* increases (see Fig. 5a). An increase in hydrogen pressure causes a mild decrease in chain growth (−0.2 order), very little of which is due to a simultaneous decrease in C* (see Fig. 5b). Increasing temperature (Fig. 5c) decreases chain growth, but like hydrogen, this change is largely unrelated to changes in C*.

Table 3
Results of least-square fits of various expressions for the rate ratio of chain growth to termination (r^*_g/r^*_t) for the C_{8+} hydrocarbons

No	Parameter	Expression	Average fractional error / %
		All dry experiments	
1	$r^*_{g,8+}/r^*_{t,8+}$	7.97	33.8
2	$r^*_{g,8+}/r^*_{t,8+}$	$15.4\theta_{C^*}$	16.0
3	$r^*_{g,8+}/r^*_{t,8+}$	$4.39\times10^{-4}\exp\{4700/T\}p_{H_2}^{-0.20}p_{CO}^{0.57}$	11.1
4	$r^*_{g,8+}/r^*_{t,8+}$	$5.66\times10^{-3}\exp\{3900/T\}\theta_{C^*}p_{H_2}^{-0.16}p_{CO}^{0.16}$	7.9
		All experiments, including water cofeed	
5	$r^*_{g,8+}/r^*_{t,8+}$	$5.82\times10^{-3}\exp\{3900/T)\theta_{C^*}p_{H_2}^{-0.21}p_{CO}^{0.21}$	12.0

The average fractional error is the standard deviation of the ratio of the fit values to the measured values.

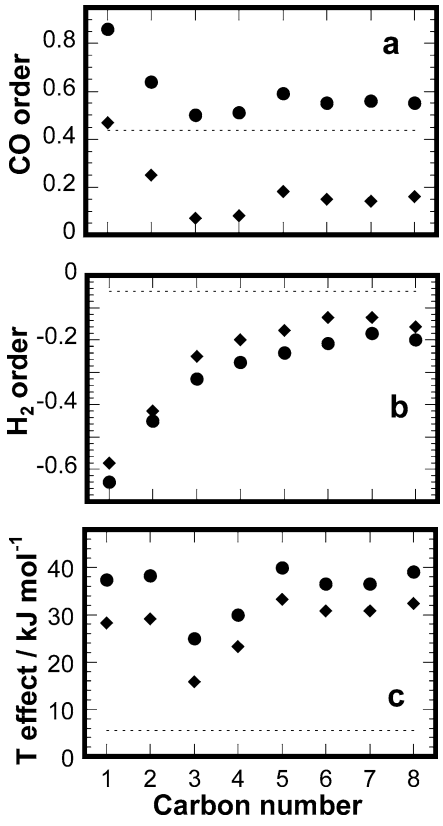

Fig. 5. Parameters from the regression fits to the C_1–C_7 hydrocarbon chain growth/termination ratios, $r^*_{g,n}/r^*_{t,n}$. (a) CO order; (b) H_2 order; (c) temperature effect (expressed as an activation energy difference). Circles show the full influence of the parameter on $r^*_{g,n}/r^*_{t,n}$. (equivalent to expression 3 in Table 3). Diamonds show the residual effect after a linear dependence on C^* has been incorporated in the fit expression (equivalent to expression 4 in Table 3). The dashed lines show the influence of the parameter on the active carbon amount, C^*, and represent the difference between the two. See text for discussion.

The low (1–4) carbon number range shows a different behavior from the higher hydrocarbon range. The change is most dramatic for methane. Chain growth at the C_1 stage has almost a first-order dependence on CO pressure (Fig. 5a) in comparison with approximately half-order for the higher hydrocarbons. The increased effect is due to changes in $k^*_{g,1}/k^*_{t,1}$. The contrast with higher hydrocarbons is consistent with the termination to an alkane, as is discussed below. This effect disappears for progressively higher carbon numbers. The effect of hydrogen (Fig. 5b) is minimal for the higher hydrocarbons, but increases smoothly with decreasing C_n until the C_1 stage is reached. At this point, hydrogen pressure decreases the probability of chain growth with greater than half-order dependence. Again, the hydrogen partial pressure dependence is almost entirely the result of changes in $k^*_{g,1}/k^*_{t,1}$. The temperature dependencies at the C_1–C_2 stage (see Fig. 5c) are similar to the asymptotic behavior for the higher hydrocarbons, despite the fact the former are dominated by alkane products and the latter by alkenes. There is a minimum in the temperature effect for C_3–C_4. Similarly to hydrogen, temperature acts directly on the rate coefficients of chain growth and termination without affecting the surface carbon coverage.

Water addition produced large simultaneous increases in both $r^*_{g,8+}/r^*_{t,8+}$ and C^*/CO. The $r^*_{g,n}/r^*_{t,n}$ values for the C_2 to C_7 hydrocarbons exhibited similar increases. For the four wet-dry experiment pairs, the average values of $\Delta\ln(r^*_{g,n}/r^*_{t,n})/\Delta\ln(C^*/CO)$ vary between 0.72 and 1.0 with carbon number and average 0.8. Therefore, the effect of water on chain growth for the lighter products can also be largely attributed to its effect on the C^* inventory. Because the effect of water vapor occurs through C^* changes, it can be argued that the residual (non-C^*-related) portion of the CO dependence noted above for C_1 is due to CO itself and not due to the water product.

4. General discussion

Both changes in C^* and changes in k^*_g/k^*_t are involved in the selectivity changes which accompany changes in reaction conditions. The syngas composition strongly affects the amounts of C^*, and thereby influences the selectivity changes indirectly. For the higher hydrocarbons, only a mild residual dependence of k^*_g/k^*_t on the syngas composition (0.15 and -0.15 order for CO and hydrogen, respectively) is unexplained by the C^* variations. On the contrary, almost all of the effect of temperature is caused by changes in k^*_g/k^*_t.

For C_1 and C_2 products, the gas-phase composition has a stronger influence on k^*_g/k^*_t than it does for the higher hydrocarbons (see Fig. 5). Differences in the termination mechanisms for the methylene–alkyl mechanism of FTS are consistent with these observed differences. In this mechanism, alkene production, dominating for C_{3+}, occurs by β-elimination of H from the growing alkyl chains, while alkane production, dominating for C_1 and C_2, requires hydrogenation of the alkyl intermediates. The chain growth step is identical for alkane and alkene products. For alkane products, naïve rate laws for chain growth and termination predict that $r^*_{g,n}/r^*_{t,n}$ is proportional to $\theta_{Cn}\theta_{C^*}/\theta_{Cn}\theta_{H^*} = \theta_{C^*}/\theta_H$. Further assumption of a simple competitive Langmuir isotherm predicts that θ_H is proportional to $P^{1/2}_{H_2}/P_{CO}$—if the surface is saturated with CO, as is the case here, and that other species (C^*, water, etc.) are not significantly involved. Thus, this simple argument predicts the gas-phase dependence in $r^*_{g,n}/r^*_{t,n}$ for alkanes to be $P^{-1/2}_{H_2}P_{CO}$. Our measurement of $P^{-0.58}_{H_2}P^{0.47}_{CO}$ for the methane product agrees well with the predicted hydrogen dependence, but the measured CO effect is substantially weaker than this prediction, though still in qualitative agreement.

A similarly simple analysis applied to alkene products predicts that $r^*_{g,n}/r^*_{t,n} \propto \theta_{C_n}\theta_{C^*}/\theta_{C_n}$ and therefore $r^*_{g,n}/r^*_{t,n} \propto \theta_{C^*}$ if there are no site requirements for H elimination. Thus no residual gas-phase influence on chain growth is predicted from this simple argument. This is also

consistent with our observations of weak residual syngas effects on chain growth for the higher hydrocarbons, which are dominated by alkenes. Even this weak residual gas-phase dependence that is observed for these products may result, in part, from the minor fraction of alkane products produced at these carbon numbers.

The similar temperature dependence for methane and the asymptotic higher hydrocarbon products is somewhat surprising, given the different termination steps for the two sets of products. A distinctive temperature effect is seen for the C_3–C_4 products (dominated by alkenes), which show a somewhat milder temperature effect than the rest of the products. Thus, for C_3 and C_4 chains, chain termination is relatively easier energetically (compared to growth) than for the higher carbon numbers. This effect probably arises from a combination of mechanism-dependent parameters, such as surface mobilities and bond energies, that cannot be resolved here.

The net chain growth rate coefficients measured in this study represent complex processes that include the effects of olefin readsorption. Olefin readsorption from a reservoir of liquid olefinic products could cause a misrepresentation of the amounts of C^*, since readsorbed olefins also undergo a degree of depolymerization [50–52], and would thus contaminate the active carbon pool. Characteristic tailing of the transient would result from such a reservoir. In addition, because of incomplete replacement of such a reservoir by ^{13}C during the transient, the forward and reverse transients would show different contributions from such a reservoir [82]. We did not observe such effects in our isotope transients. This is likely because they were obtained at low CO conversion and the resulting product partial pressures/activities are relatively low. There is a mild trend to higher C^* amounts with higher syngas pressure, but this trend saturates in our data (see the sequence c, d, e, and f, for example) in the presence of increasing activities and increasing olefin fractions. Therefore, the C^* amounts measured here are true measures of the surface species.

Although alkene readsorption does not affect our C^* measurements, rapid reversibility can have an influence on the measured chain growth parameters. The measured $r^*_{g,n}/r^*_{t,n}$ ratios are *net* values (forward–reverse) and thus contain the effects of readsorption (reverse termination) and depolymerization (reverse chain growth). Furthermore, if chain growth were to be very rapidly reversible, the fraction of the active carbon in the form of growing chains (rather than as monomeric species) could be substantial. Previous steady-state tracer studies indicate that under low conversion conditions, the rate of polymerization is substantially faster than depolymerization [45,51,55]. For example, in Ref. [51], the rate of polymerization of readsorbed ethene and hexene on Ru was 4–5 times faster than depolymerization. On this basis, the reversibility of chain growth would appear to be small; however, a direct measurement under the conditions of this study is necessary to confirm this quantitatively. Readsorption and a finite probability of termination to the alkane product are believed to be the key processes that leads to an alkane fraction in the product that increases with carbon number and with conversion [7,47]. By decreasing the net chain termination rate, the readsorption process alters the carbon number distribution. Extensive models of the Fischer–Tropsch reaction that include such processes have shown the important effect they have on the product distribution [4,7,45]. We emphasize that under our low conversion conditions, alkenes dominate our measured C_3–C_7 product distribution due to the short residence times. Thus, while olefin readsorption does not affect the validity of our analysis, it may still be an influencing factor on the lumped rate coefficient ratios obtained in this study. More complete modeling of such effects is reserved for future studies.

5. Conclusions

Based on our isotope transient kinetic studies of the selectivity-governing processes of cobalt-catalyzed FTS we have concluded that under industrially relevant conditions:

- The rate ratio of propagation to termination during chain growth in FTS on cobalt is strongly correlated with the steady-state amount of active surface carbon for all carbon number products. An approximately linear dependence supports the notion that the dominant form of active carbon under reaction conditions is monomeric.
- Most of the effects of changes in CO and, particularly, water partial pressures on the chain growth probability appear to arise via an indirect effect on the active carbon inventory.
- H_2 and CO have at most a mild residual direct influence on chain growth to alkene products and a stronger influence on the termination probability to alkanes.
- Temperature has little effect on C^* inventories and affects chain growth directly through the surface rate coefficients.

Acknowledgments

The authors gratefully acknowledge the generous supply of catalyst by Dr. Andre Malek and the technical assistance of Mr. Gregory J. DeMartin in constructing the high pressure transient kinetic unit, both of ExxonMobil Research and Engineering Co. C.A.M. and C.J.B. thank ExxonMobil Research and Engineering Co. for research support.

References

[1] T.H. Fleisch, R.A. Sills, M.D. Briscoe, J. Nat. Gas Chem. 11 (2002) 1.
[2] M.E. Dry, Catal. Today 71 (2002) 227.
[3] B.H. Davis, Fuel Process. Technol. 71 (2001) 157.
[4] G.P. van der Laan, A.A.C.M. Beenackers, Catal. Rev.-Sci. Eng. 41 (1999) 255.
[5] G.P. van der Laan, A.A.C.M. Beenackers, Ind. Eng. Chem. Res. 38 (1999) 1277.

[6] H. Schulz, Appl. Catal. A 186 (1999) 3.
[7] E. Iglesia, Appl. Catal. A 161 (1997) 59.
[8] E. Iglesia, S. Reyes, R.J. Madon, S.L. Soled, Adv. Catal. 39 (1993) 221.
[9] R.B. Anderson, The Fischer–Tropsch Synthesis, Academic Press, New York, 1984.
[10] P.J. van Berge, Stud. Surf. Sci. Catal. 107 (1997) 207.
[11] R.L. Espinoza, A.P. Steynbert, B. Jager, A.C. Volsloo, Appl. Catal. A 186 (1999) 13.
[12] W. Conner, T.K. Das, G. Jacobs, L. Li, B.H. Davis, in: AIChE Prepr. Spring Natl. Meeting, 2003, p. 2694.
[13] S. Krishnamoorthy, M. Tu, M.P. Ojeda, D. Pinna, E. Iglesia, J. Catal. 211 (2002) 422.
[14] M. Claeys, E. van Steen, Catal. Today 71 (2002) 419.
[15] C.J. Bertole, C.A. Mims, G. Kiss, J. Catal. 210 (2002) 84.
[16] A.M. Hilmen, O.A. Lindvag, E. Bergene, D. Schanke, S. Eri, A. Holmen, Stud. Surf. Sci. Catal. 136 (2001) 295.
[17] H. Schulz, M. Claeys, S. Harms, Stud. Surf. Sci. Catal. 107 (1997) 193.
[18] H. Schulz, E. van Steen, M. Claeys, Stud. Surf. Sci. Catal. 81 (1994) 455.
[19] C.J. Kim, US patent 5,227,407, 1993.
[20] H.P. Withers, K.F. Eliezer, J.W. Mitchell, Ind. Eng. Chem. Res. 29 (1990) 1807.
[21] C.J. Kim, European patent 0,339,923, 1989.
[22] E. Iglesia, R. Madon, US patent 4,754,092, 1988.
[23] A.M. Hilmen, D. Schanke, K.F. Hanssen, A. Holmen, Appl. Catal. A 186 (1999) 169.
[24] F.M. Gottschalk, R.G. Copperthwaite, M. van der Riet, G.J. Hutchings, Appl. Catal. 38 (1988) 103.
[25] P.J. van Berge, J. van de Loosdrecht, S. Barradas, A.M. van der Kraan, Catal. Today 58 (2000) 321.
[26] D. Schanke, A.M. Hilmen, E. Bergene, K. Kinnari, E. Rytter, E. Adnanes, A. Holmen, Energy Fuels 10 (1996) 867.
[27] Y. Zhang, D. Wei, S. Hammache, J.G. Goodwin Jr., J. Catal. 188 (1999) 281.
[28] M. Rothaemel, K. Firing-Hanssen, E.A. Blekkan, D. Schanke, A. Holmen, Catal. Today 8 (1997) 79.
[29] J.K. Minderhoud, M.F.M. Post, S.T. Sie, S.T.S Sudholter, US patent 4,628,133, 1986.
[30] S.B. Craxford, E. Rideal, Brennstoff-Chem. 20 (1939) 263.
[31] A.T. Bell, Catal. Rev.-Sci. Eng. 23 (1981) 203.
[32] R.A. Friedel, R.B. Anderson, J. Am. Chem. Soc. 72 (1950) 1212, 2307.
[33] R. Brady, R. Pettit, J. Am. Chem. Soc. 102 (1980) 6181.
[34] R. Brady, R. Pettit, J. Am. Chem. Soc. 103 (1980) 1287.
[35] I.M. Ciobica, G.J. Kramer, Q. Ge, M. Neurock, R.A. van Santen, J. Catal. 212 (2002) 136.
[36] W.S.B. Ndlovu, N.S. Phala, M. Hearshaw-Timme, P. Beagly, J.R. Moss, M. Claeys, E. van Steen, Catal. Today 78 (2003) 581.
[37] Z.-P. Liu, P. Hu, J. Am. Chem. Soc. 124 (2002) 11568.
[38] P.M. Maitlis, R. Quyoum, H.C. Long, M.L. Turner, Appl. Catal. A 186 (1999) 363.
[39] M.J. Overett, R.O. Hill, J.R. Moss, Coord. Chem. Rev. 206 (2000) 581.
[40] R. Quyoum, V. Berdini, M. Turner, H.C. Long, P.M. Maitlis, J. Am. Chem. Soc. 118 (1996) 10888.
[41] G. Henrici-Olive, S. Olive, J. Mol. Catal. 16 (1982) 111.
[42] J.J.C. Geerlings, M.C. Zonnevylle, C.P.M. De Groot, Surf. Sci. 241 (1991) 302.
[43] R.J. Madon, E. Iglesia, J. Mol. Catal. A: Chem. 163 (2000) 189.
[44] H. Schulz, M. Claeys, Appl. Catal. A 186 (1999) 71.
[45] H. Schulz, M. Claeys, Appl. Catal. A 186 (1999) 91.
[46] G.P. van der Laan, A.A.C.M. Beenackers, Stud. Surf. Sci. Catal. 119 (1998) 179.
[47] E.W. Kuipers, I.H. Vinkenburg, H. Oosterbeek, J. Catal. 152 (1995) 137.
[48] R.J. Madon, E. Iglesia, J. Catal. 139 (1993) 576.
[49] E. Iglesia, S.C. Reyes, R.J. Madon, S.L. Soled, Adv. Catal. 39 (1993) 221.
[50] K.R. Krishna, A.T. Bell, Catal. Lett. 14 (1992) 305.
[51] C. Mims, J. Krajewski, K. Rose, M.T. Melchior, Catal. Lett. 7 (1990) 119.
[52] Y. Kobori, H. Yamasaki, S. Naito, T. Onishi, K. Tamaru, J. Chem. Soc., Faraday Trans. (1982) 1473.
[53] H. Pichler, H. Schulz, Chem.-Ing.-Tech. 42 (1970) 1162.
[54] G.V. Isagulyants, N.I. Ershov, Y.I. Derbentsev, Y.T. Eidus, Isv. Adad. Nauk SSSR, Ser. Khim. 6 (1968) 1234.
[55] Y.T. Eidus, Usp. Khim. 36 (1967) 824.
[56] D.J. Klinke, L. Broadbelt, J. Chem. Eng. Sci. 54 (1999) 3379.
[57] E. Iglesia, S.L. Soled, J.E. Baumgartner, S.C. Reyes, Top. Catal. 2 (1995) 17; J. Catal. 153 (1995) 108.
[58] L. Nowicki, S. Ledakowicz, D.B. Bukur, Chem. Eng. Sci. 56 (2001) 1175.
[59] M.N. Yakubovich, Pisarzhevskovo, Zh. Fiz. Khim. 76 (2002) 2145.
[60] G. Huff Jr., C.N. Satterfield, J. Catal. 85 (1984) 370.
[61] L. Konig, J. Gaube, Chem.-Ing.-Tech. 55 (1983) 14.
[62] B. Sarup, B.W. Wojciechowski, Can. J. Chem. Eng. 66 (1988) 831.
[63] B.W. Wojciechowski, Can. J. Chem. Eng. 64 (1986) 149.
[64] J. Patzlaff, Y. Liu, C. Graffmann, Gaube, J. Appl. Catal. A 186 (1999) 109.
[65] P. Biloen, J.N. Helle, F.G.A. van den Berg, W.M.H. Sachtler, J. Catal. 81 (1983) 450.
[66] X. Zhang, P. Biloen, J. Catal. 98 (1986) 468.
[67] C.A. Mims, L.E. McCandlish, J. Phys. Chem. 91 (1987) 929.
[68] K.R. Krishna, A.T. Bell, J. Catal. 139 (1993) 104.
[69] T. Komaya, A.T. Bell, Z. Weng-Sieh, R. Gronsky, F. Engelke, T.S. King, M. Pruski, J. Catal. 150 (1994) 400.
[70] S.L. Shannon, J.G. Goodwin Jr., Chem. Rev. 95 (1995) 677.
[71] K.F. Hanssen, E.A. Blekkan, D. Schanke, A. Holmen, Stud. Surf. Sci. Catal. 109 (1997) 193.
[72] H.A.J. van Dijk, J.H.B.J. Hoebink, J.C. Schouten, Chem. Eng. Sci. 56 (2001) 1211.
[73] H.A.J. van Dijk, PhD thesis, Technische Universiteit Eindhoven, Eindhoven, Netherlands, 2001.
[74] F. Rohr, O.A. Lindvag, A. Holmen, E.A. Blekkan, Catal. Today 58 (2000) 247.
[75] A.R. Belambe, R. Oukaci, J.G. Goodwin Jr., J. Catal. 166 (1997) 8.
[76] C.A. Mims, C.J. Bertole, Stud. Surf. Sci. Catal. 136 (2001) 375.
[77] C.A. Mims, C.J. Bertole, G. Kiss, P.V. Joshi, Stud. Surf. Sci. Catal. 136 (2001) 369.
[78] C.J. Bertole, C.A. Mims, G. Kiss, J. Catal. 221 (2004) 191.
[79] C.J. Bertole, PhD thesis, University of Toronto, Toronto, Canada, 2002.
[80] C.H. Mauldin, D.E. Varnado, Stud. Surf. Sci. Catal. 136 (2001) 417.
[81] E.F.G. Herrington, Chem. Ind. 65 (1946) 346.
[82] Y. Soong, K. Krishna, P. Biloen, J. Catal. 97 (1986) 330.